High-temperature preparation of Ni_2P suspended within carbon matrix and its potential as HER electrocatalyst

Nataliia Reinders[1]*, Martin Ďurovič[2], Pavla Honcová[1], Žaneta Dohnalová[1], Jana Luxová[1], Stanislav Slang[3], Jhonatan Rodriguez-Pereira[3,4], Petra Šulcová[1].

[1]Department of Inorganic Technology, Faculty of Chemical Technology, University of Pardubice, Studentská 95, 532 10, Pardubice, Czech Republic

[2]Department of Inorganic Technology, University of Chemistry and Technology, Prague, Technická 5, 166 28, Prague 6, Czech Republic

[3]Center of Materials and Nanotechnologies, Faculty of Chemical Technology, University of Pardubice, nám. Čs. legií 565, 530 02 Pardubice, Czech Republic

[4]Central European Institute of Technology, Brno University of Technology, Purkyňova, 123, 612 00 Brno, Czech Republic

*Corresponding author: tel. +420 466 037 182; e-mail nataliia.reinders@upce.cz

Abstract

Hydrogen production via electrocatalytic reduction of water is a promising clean-energy technology. For further advancement of this technology, the exploration of cost-effective and streamlined approaches for producing active phosphide-based catalysts is of great importance. This study presents a new high-temperature preparation method of a microporous Ni_2P/C catalyst composed of crystalline Ni_2P nanoparticles homogeneously distributed within an amorphous carbon matrix in a weight ratio of 40/60. The redox transformation leading to the formation of Ni_2P from not-reduced stable inorganic salts was facilitated during thermal treatment by a polymeric precursor, which, in turn, transformed into microporous carbon matrix that prevented the newly formed phosphide particles from agglomerating and sintering. The microporous structure of the prepared composite was characterised by gas adsorption technique and modelled using density functional theory and statistical thickness methods. The t-plot revealed high micropore surface area of 333.5 $m^2\ g^{-1}$ (accounting 97 % of total surface area) and the pore size distribution in the range of 10-12 Å. According to TEM analysis, the size range of the Ni_2P inclusions varied from 5 to 200 nm. The evaluation of electrocatalytic properties of the Ni_2P/C composite demonstrated its high HER activity and stability under high voltages in alkaline water electrolysis conditions. Furthermore, HER activity of the composite was substantially enhanced by grinding, which opened closed microporosity channels and increased the micropore surface area to 355.2 $m^2\ g^{-1}$, thereby increasing the number of catalytically active sites in the sample. The result indicates the exceptional role of the microporous microstructure of the composite in its catalytic performance. The findings of this study may have a significant impact on the practical implementation of efficient hydrogen production by water electrolysis.

Keywords

Nickel (II) phosphide, amorphous carbon matrix, microporous composite, polymeric precursor method, hydrogen production

1 Introduction

In recent years, transition metal phosphides (TMP) have been the focus of intense investigations due to their unique structural characteristics and potential applications in various areas, including hydrogen production through alkaline water electrolysis[1–8]. Among the TMPs, nickel (II) phosphide (Ni_2P) was reported to have one of the highest activities for the hydrogen evolution reaction (HER) of

any non-noble metal electrocatalyst, producing hydrogen with nearly quantitative faradaic yield[9]. However, TMPs still have some limitations, such as a lack of chemical stability at a high current density and limited exposure of electrocatalytic active sites, which prevent them from meeting the benchmark of noble metal catalysts.

Efforts to improve the efficiency of Ni_2P electrocatalysts have focused on modifying its chemical composition or hybridising it with other materials[6,7,10–18]. Hybridisation of Ni_2P with a conductive material, such as graphene, carbon or carbon nitride, enhanced not only the catalytic activity by improving the overall conductivity of the composite but also the electrode stability at a high current density by preventing agglomeration of Ni_2P clusters in a fast electron transfer process. Furthermore, the carbonaceous matrix with an advantageous hydrophilic and aerophobic surface can provide a low ohmic resistive path at the electrode−electrolyte interface. At the same time, its porous architecture can accelerate the diffusion of gas bubbles from the electrode surface, thereby minimising its dead area[7,13].

The strategy of Ni_2P hybridisation with carbonaceous materials has also been successfully applied in other areas, such as the photocatalytic production of H_2 using solar cells and electrochemistry[2,13,19–21]. The unique microstructure of these composites contributed to the superior electrochemical performance of hybridised TMP electrodes by ensuring a uniform distribution of the phosphide, improving conductivity, interfacial interaction and charge separation, increasing surface area and providing a buffer zone that accommodated volume expansion during charging/discharging. All these reports underline the undoubtful advantages of carbonaceous composite materials as compared with pure TMPs, which are evident in the wide application range.

However, the synthesis process of such hybridised materials is very complex and usually requires utilisation of hypophosphites or even phosphorus as the starting compound[2,4,5,7,14,16,19–22]. Therefore, the development of an alternative preparation method using stable and affordable starting compounds would be of great importance from a practical point of view.

In this work, the hybridisation of nickel (II) phosphide with an amorphous carbon matrix was conducted using basic inorganic salts and an undemanding synthesis approach based on the polymeric precursor method. The elaborated method provided the formation of a highly efficient and stable electrocatalyst for the water splitting reaction. In addition to the general characterisation of the obtained catalyst, including HER electrocatalytic activity, the thermal stability of the product in different atmospheres is the focus of this paper.

2 Materials and Methods

2.1 Synthesis

The sample was obtained by pyrolysis in an N_2 atmosphere of a polymeric precursor containing nickel (II) and phosphate. The polymeric precursor was obtained as follows. Solutions of $Ni(NO_3)_2{\cdot}6H_2O$ and $NH_4H_2PO_4$ were used as sources of nickel and phosphate; citric acid $C_3H_5OH(COOH)_3$ and ethylene glycol $(CH_2OH)_2$ were used as initial reagents for polymer formation. The Ni^{2+} solution was mixed with citric acid in a 1:4 molar ratio for 2 h at 300 rpm on a magnetic stirrer. Then ethylene glycol (EG:CA = 4:1) and phosphate (Ni:P = 3:2) solutions were added and the stirring rate was increased to 500 rpm and. In 1 h, the mixture was gradually heated from room temperature to 75 ^{o}C on a magnetic stirrer coupled with a heating plate for 6 h, resulting in the formation of a viscous, transparent gel. The gel was dried for several days in a laboratory dryer with a gradual increase in temperature from 75 to 150 ^{o}C. During the drying process, the bright green gel first transformed into yellow-brown sticky gum that, with time, completely solidified and transformed into a hard brown polymer (polymeric precursor). The polymer precursor was dried until its weight reduction was stopped. Calcination of the

polymer precursor was carried out in a tube furnace in an inert atmosphere (50 ml min^{-1} N_2 flow) at 1000 °C for 2 h with a heating rate of 5 °C min^{-1}. Small amount of the sample was ground in an agate grinding container with agate balls (30 pieces, 10 mm in diameter) with addition of ethanol using a planetary mill (Fritsch Pulverisette) for 30 min with an oscillation of 30-60 s^{-1}.

2.2 Methods

Phase composition analysis was performed by powder XRD using a Miniflex 600 benchtop diffractometer (Rigaku, JAP, CuK_α radiation, CuK_β Ni filter, 1D detector D/teX Ultra, continuous scanning over the 2theta range from 10 to 80° with scanning speed of 5-10° 2theta min^{-1}, recorded step size 0.02° 2theta). Phase identification was performed using PDXL2 Rigaku data analysis software by searching for a match in the PDF-2 database. The quantitative composition of the crystalline part of the multiphase samples was calculated on the basis of RIR analysis using PDXL2 software.

A scanning electron microscope (Lyra 3, Tescan) was used at an accelerating voltage of 10 kV to study the surface morphology of the composite. SEM images were recorded using SE and BSE detectors at a working distance of 7 mm. The chemical composition of the composite was studied by energy dispersive X-ray spectroscopy (EDS/EDX) using an Aztec X-Max 20 system (Oxford Instruments) attached to SEM (Lyra 3, TESCAN) with an acceleration voltage of 5 kV.

TEM observation was performed by Jeol 2200 FS (TEM, Jeol, Japan; Schottky emitter, point resolution 0.23 nm) equipped with TVIPS camera (Munich, Germany) and EDS analyser (EDS, Oxford Instruments, Abingdon, UK).

The surface chemical composition analysis was performed by X-ray photoelectron spectroscopy (XPS) on a Scienta-Omicron ESCA2SR system using a monochromatic Al Kα X-ray source (1486.6 eV) operated at 100 W. Correction of the binding energy scale was done using the sp^2 carbon signal at 284.0 eV. Quantitative analysis was performed using the elemental sensitivity factors provided by the manufacturer.

The thermal transformation of the polymeric precursor and the thermal stability of the final product in inert and oxidising atmospheres (Ar or airflow, 50 ml min^{-1}) was studied using thermal analysis (DSC-TGA, Labsys Evo 1600, Setaram, FR). Measurements were carried out in corundum crucibles in a temperature range of 25-1200 °C with a heating rate of 10 °C min^{-1}.

The surface area and porosity of the samples were analysed using a Quantachrome NovaWin physisorption analyser (Quantachrome Instruments, Anton Paar Quanta Tec Inc., USA) under the following conditions: analysis gas N_2 (adsorbate), analysis temperature 77.35 K, pressure tolerance 0.1/0.1 (ads/des), equilibrium time 90/90 s (ads/des), equilibrium timeout 240/240 s (ads/des). Samples were analysed after outgassing for 3 h at 200 °C. The micropore volume was calculated on the basis of the statistical thickness (t-plot) using MP analysis methods. The pore size distribution was calculated using MP analysis method and the density functional theory, DFT (nonlocal DFT equilibrium model for N_2 at 77 K on carbon; slit and cylindrical pore geometry were assumed for the pores below and above 2 nm, respectively).

The stability of the sample to acid and bases was tested in HCl (35%), HNO_3 (65%), aqua regia and NaOH (30%). For the test, 0.1 g of the sample was treated in 25 ml of liquid for 48 h at room temperature; the effect of heating to 50 °C in the corrosive environment was also studied.

The density of the samples before and after grinding was determined using a gas displacement pycnometer (AccuPyc 1320, Micromeritics, USA, gas – He, each sample measured at least 10 times). The weight of the evaluated samples ranged from 2 to 3 g.

Electrochemical activity and stability of the samples were determined by (i) measurements of the polarisation curves - evaluation of the Tafel equation (Tafel slope, exchange current density, and overpotential at current densities of 10 and 300 mA cm^{-2}) and (ii) electrochemical impedance spectroscopy (EIS) - evaluation of ohmic and polarization resistances at selected electrode potentials.

Measurements of the polarisation curves were performed on a rotating disk electrode (RDE) at 30 °C in 0.1 mol dm^{-3} KOH solution over a range of current densities from 0 to −10 mA cm^{-2} with a scan rate of 2 µA s^{-1} cm^{-2}. Ni wire was used as a counter electrode and reversible hydrogen electrode (RHE) was used as a reference electrode. All potentials presented in the article are IR-corrected. The rotation speed of the disk electrode was set to 500 rpm to ensure a sufficiently fast removal of the bubbles. A N_2 atmosphere was maintained throughout the measurements above the nitrogen saturated solution. A catalyst ink contained 10 mg of the selected catalyst, 10 µl of an anion-selective binder Fumion and 5 ml of water. A volume of 20 µl of homogeneous catalyst ink was pipetted onto the glassy carbon (0.196 cm^2) electrode in two steps. After the water evaporated, the electrode was ready for measurement. Prior to the actual measurement of the polarisation curves and EIS, the electrodes were activated/stabilised by cyclic voltammetry (100 cycles in the range of 0 to −10 mA cm^{-2}). For each sample, 2 to 3 RDEs were prepared and measured. For comparison purposes, RDEs with a commercial Pt/C catalyst (40%wt, Alfa Aesar) and commercial Ni powder (50 µm, 99.7% purity, Sigma-Aldrich), prepared by the above-mentioned method, were used.

EIS spectra were measured over a frequency range of 100 kHz to 0.1 Hz with an amplitude of 20 mV at potentials of −0.25; −0.3; −0.35; −0.4 and −0.5 V vs. RHE under the same conditions as polarisation curve measurements. An equivalent circuit (Fig. 1) consisting of Rs (ohmic resistance of the electrolytic cell), Rp (HER polarisation resistance) and CPE (constant phase element, double-layer capacitance at the interface between an electrode and electrolyte) was used to evaluate the spectra.

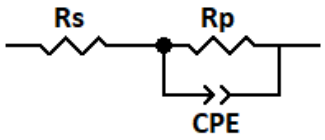

Figure 1. Equivalent circuit used to evaluate EIS spectra. Rs (ohmic resistance), Rp (polarisation resistance) a CPE (constant phase element).

The stability testing procedure of the ground Ni_2P consisted of three individual steps. First, the polarisation curve was measured and the Tafel parameters were determined. Then, electrochemical impedance spectroscopy was measured at different voltages, which was used to evaluate the polarisation and ohmic resistances. In the last step, the cyclic voltammetry (500 cycles, from 0 to −0.4 V vs RHE, 100 mV s^{-1}) was performed. Since this is an established stability testing procedure, the measurements were performed in potentiostatic mode[23]. The whole procedure was repeated three times and the change of above-mentioned parameters with respect to the number of cycles was evaluated.

3 Results and Discussion

3.1 Formation and characterisation of the Ni_2P/C composite

The formation of nickel (II) phosphide dispersed within an amorphous carbon matrix (Ni_2P/C) is successfully achieved by the polymeric precursor method utilising basic inorganic salts ($Ni(NO_3)_2 \cdot 6H_2O$ and $NH_4H_2PO_4$) as initial compounds. XRD analysis of the product indicates a pure well crystalline Ni_2P phase (ICDD 01-074-1385) (Figure 2, the product after treatment at 1000 °C for 2 h). The XRD pattern also shows a weak halo centred at 20° 2theta which indicates an amorphous phase attributed to

carbon. The amorphous carbonaceous component is also clearly identified by SEM micrographs (Fig. 3), showing the crystalline phosphide particles as light spheres and the amorphous carbon as a dark porous matrix. The SEM images show that the Ni_2P particles are about 200 nm in size and are individually isolated from each other by a solid carbon matrix (Fig. 3). In addition, the carbon matrix exhibits circular openings that align closely in size with the phosphide particles (approx. 200 nm), suggesting that these openings likely housed the phosphide particles that were detached during the grinding process. The abundance and uniform distribution of phosphide inclusions on the surface of the grinded composite imply their even dispersion throughout the volume of the carbon matrix. Further insights into the sample's microstructure and elemental arrangement were conducted through a TEM-EDS analysis. The EDS analysis conclusively confirmed the co-localization of P and Ni atoms within the inclusions attributed to the nickel phosphide phase (Fig 4a). Furthermore, the TEM analysis demonstrated the intricate integration of nano-sized nickel phosphide within the surrounding matrix primarily composed of carbon (Fig. 4b). The observations indicate a notable variation in the size of the Ni_2P inclusions within the composite, spanning a range from 5 to 200 nm.

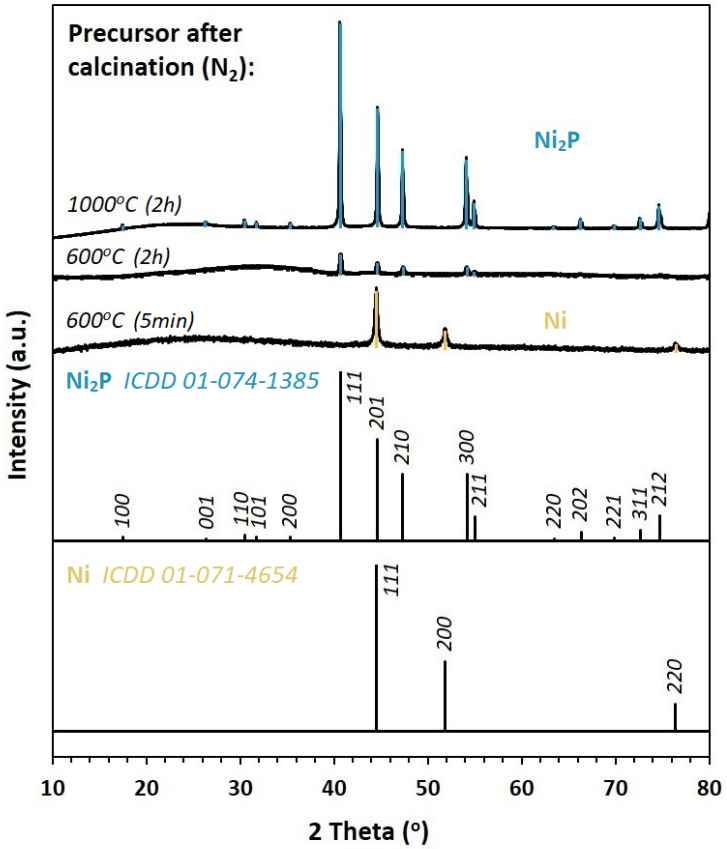

Figure 2. XRD analysis of the polymeric precursor after treatment at 600 °C (for 5 min and 2 h) and 1000 °C (for 2 h).

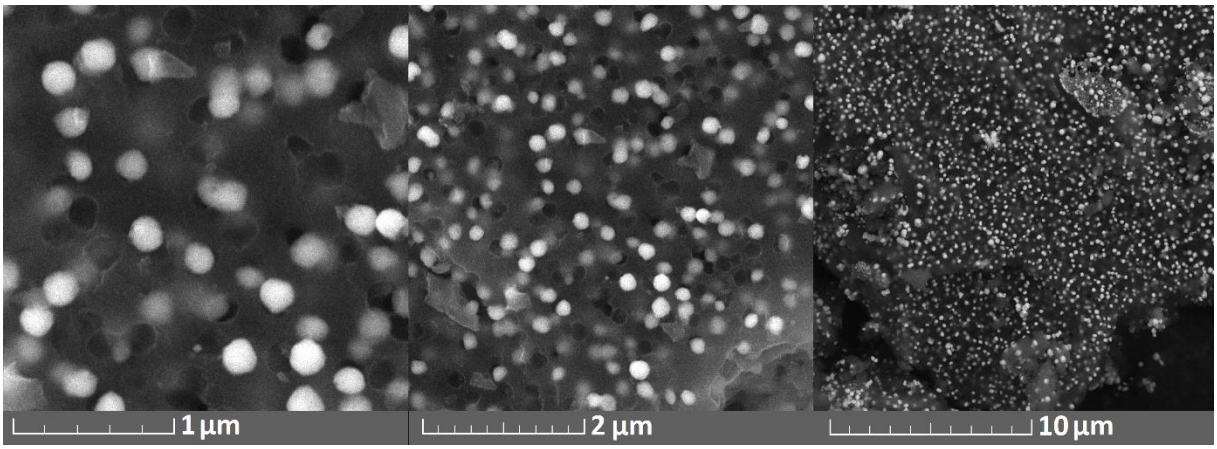

Figure 3. SEM micrographs of the Ni_2P/C composite showing uniformly distributed Ni_2P crystalline phosphide (light spheres) suspended within an amorphous carbon matrix (dark porous matrix).

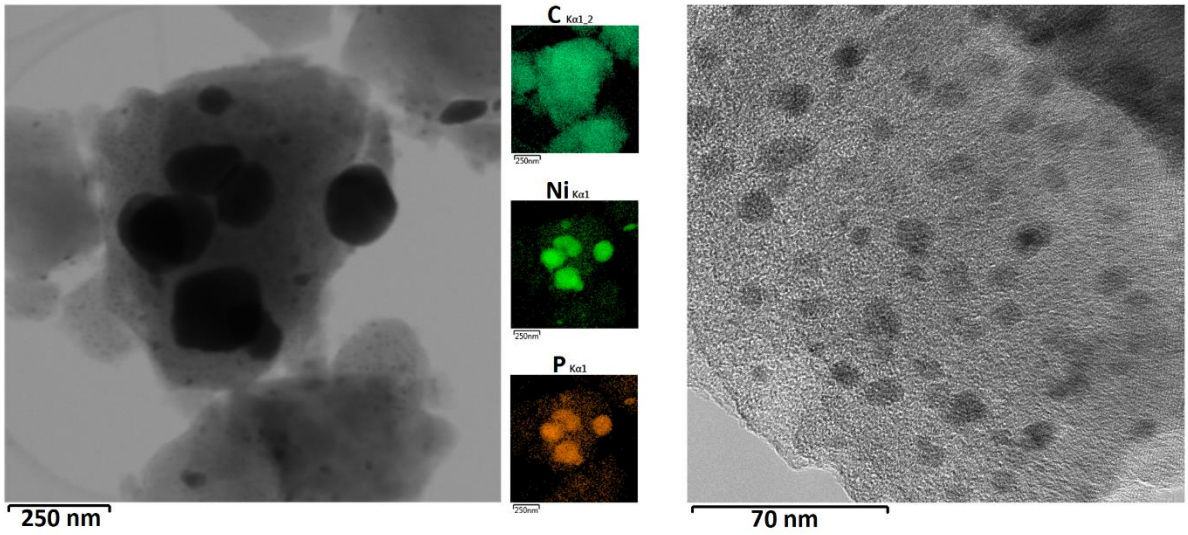

Figure 4. TEM analysis of the Ni_2P/C composite: (a) visualisation and elemental mapping of carbon (C), nickel (Ni), and phosphorus (P) elements; (b) in-depth visualisation of the carbon matrix intricately integrated with nanoparticles.

According to the EDX analysis, the Ni_2P/C composite comprises 59.5%wt (81.1%at) of C, 24.7%wt (6.9%at) of Ni, 8.3%wt (4.4%at) of P and 7.3%wt (7.5%at) of O. Supplementary information on the surface composition of the composite is provided by XPS analysis (Supplement 1). According to the C *1s* high-resolution spectrum deconvolution, most carbon bonds are identified as sp^2 hybridised species (284.0 eV), next to some sp^3 hybridised bonds (284.8 eV), single C—O bonds (286.1 eV), double carbonyl bonds C=O (287.9 eV) and (C=O)-OH (289.3 eV), and a contribution of π-π* shake-up satellite (290.6 eV). The XPS analysis of Ni *2p* confirms the presence of two different chemical species. Ni—P bonds with the corresponding spin-orbit splitting Ni $2p^{3/2}$ and Ni $2p^{1/2}$ centred at 853.2 eV and 870.5 eV (Supplement 1, red peaks) are associated with Ni_2P. The second doublet (Supplement 1, blue peaks) evidences the presence of Ni-O bonds (857.0 and 874.5 eV). The third doublet (Supplement 1, green peaks) is related to shake-up satellites. P *2p* spectrum also exhibits two chemical environments: Ni—P species with the doublets (P $2p^{3/2}$ and P $2p^{1/2}$ at 129.5 and 130.3 eV, respectively), confirming the presence of Ni_2P (Supplement 1, red peaks), and P-O bonds (Supplement 1, blue peaks) centred at 133.3 and 134.1 eV. The signal of O *1s* shows mainly bonds with P and Ni at 531.2 eV and organic

oxygen at 532.8 eV. The high content of oxygen and the presence of the oxidized bonds on the surface could indicate either surface oxidation, which is typical for metal phosphides once exposed to open air[4,11,24], or presence of an additional amorphous component of nickel (II) phosphate, which is impossible to detect by XRD. For example, XPS spectra and an XRD pattern similar to those reported here were observed for another hybrid material composed of an amorphous nickel (II) phosphate matrix and crystalline Ni_2P particles[25]. Therefore, the possible presence of amorphous nickel (II) phosphates in our sample must be verified by complementary techniques, such as FTIR method and XRD analysis of the heated sample[25]. The FTIR study of our sample (Supplement 2) does not show any signs of phosphate groups that typically appear in the fingerprint region between 900 and 1100 cm^{-1} [26]. Moreover, thermal treatment of the sample in an inert atmosphere does not result in crystallisation of a new phosphate phase (discussed in detail in the next section), which also confirms the absence of an amorphous phosphate in the synthesised composite.

Thermal transformation of the polymeric precursor and the formation of the Ni_2P/C composite is characterised by the combination of DSC-TGA, powder XRD and SEM techniques. After the preliminary drying stage at 150 °C, the polymeric precursor consists of an amorphous solidified fragile resin (Fig. 5 SEM image from the left). During heating in an inert atmosphere, a substantial weight loss of almost 70% that appears on the TGA curve between 300 and 400 °C attributed to the pyrolysis of the polymer (Fig. 5, red curve). During the process, the sample is significantly reduced in volume and fragmented into smaller pieces (Fig. 5, SEM image in the middle). The XRD pattern of the sample heated at 600 °C shows several weak reflections corresponding to a crystalline phase of metal Ni, ICDD 01-071-4654 as well as a halo centred at 20° 2theta corresponding to an amorphous phase (Fig. 5), neither of which can be recognised on the SEM image of this sample. Most likely, the reduction of Ni^{2+} to Ni^0 occurs during the redox interaction between the inorganic and organic components. The possibility of Ni^{2+} reduction by ethylene glycol alone is known as the polyol process, which is based on the decomposition of ethylene glycol and its conversion to diacetyl above its refluxing temperature[27]. On the DSC curve (Fig. 5, grey curve), the beginning of the pyrolysis process at 300 °C is indicated by an endothermic decrease that changes to exothermic at higher temperatures. In fact, pyrolysis of a polymer is a heat-consuming process[28], but in the studied case it is overlapped by exothermic redox reaction between Ni^{2+} and unreacted ethylene glycol, which could remain in the mixture and act as a reducing agent with heating. Further, metallic Ni promptly reacts with the phosphate component to form Ni_2P (ICDD 01-074-1385), the weak diffractions of which can be well recognised on the XRD pattern of the sample after prolonged heating at 600 °C (Fig. 2, the product after treatment at 600 °C for 2 h). With a further temperature increase, an additional step-like weight loss of 20% appears between 700 and 800 °C. After calcination at 1000 °C for 2 h, the only crystalline phase detected in the product corresponds to Ni_2P (ICDD 01-074-1385) (Fig. 2). During the transformation, the appearance of the sample also dramatically changes: its smooth polymer-like consistency is fractured and textured, clearly showing two different components of an amorphous matrix and crystalline particles (Fig. 5, SEM images from the right with different magnifications).

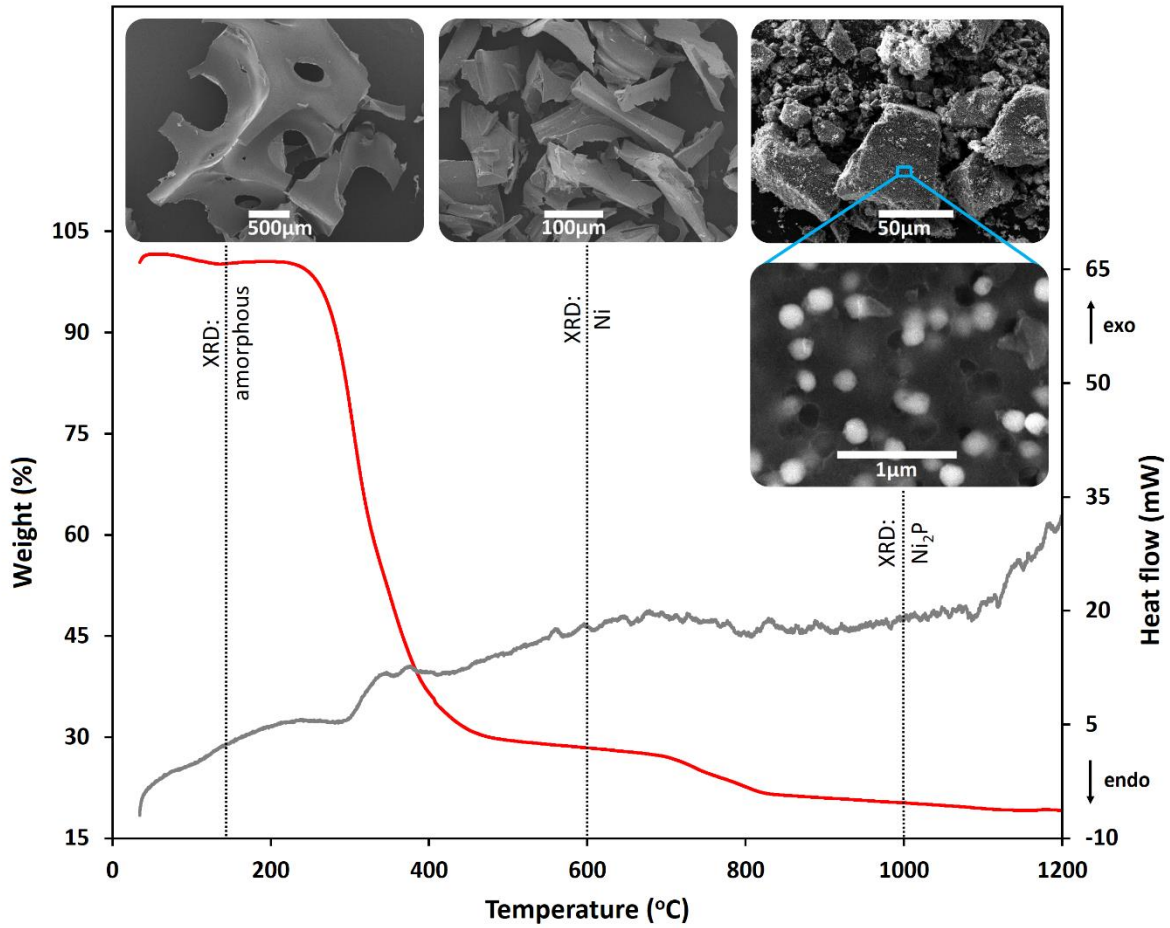

Figure 5. Transformation of the polymeric precursor into the Ni_2P/C composite studied by DSC-TGA; SEM images correspond to the polymeric precursor dried at 150 °C in the open air (from the left) and the precursor heated in an inert atmosphere at 600 °C (in the middle) and 1000 °C (from the right).

The developed synthesis approach based on the polymeric precursor method allows fabrication of fine Ni_2P particles dispersed within an amorphous carbon matrix using stable and affordable inorganic salts ($Ni(NO_3)_2{\cdot}6H_2O$ and $NH_4H_2PO_4$) as initial compounds. Traditionally, the Ni_2P/C composites were synthesised by phosphorylation of the Ni-based metal-organic framework using phosphorus or hypophosphites[2,4,5,7,14,16,19–22]. Only a few publications reported the utilisation of inorganic phosphate as the initial compound for Ni_2P synthesis by either the temperature-programmed reduction method[29,30] or pyrolysis followed by surface phosphidation with sodium hypophosphite [18]. On the other hand, phosphate salts were extensively used as typical starting compounds for the synthesis of nickel (II) phosphates[31,32]. In particular, the polymeric precursor method was used for the synthesis of pure inorganic phosphate, $Ni_3(PO_4)_2$, using the same initial compounds as in the present study[31]. However, the formation of $Ni_3(PO_4)_2$ also involved a redox interaction that led to the crystallisation of Ni_2P as an intermediate product, which then transformed under heating in an oxidising atmosphere to $Ni_3(PO_4)_2$. This underlines the unique role of the polymer, which acts as a reduction agent in the mixture and induces redox processes leading to the formation of Ni_2P, both in oxidising and inert atmospheres. On the other hand, the type of atmosphere determines the subsequent behaviour of the formed phosphide: either its oxidation to $Ni_3(PO_4)_2$ in an oxidising atmosphere or the maintenance of the Ni_2P structure in an inert atmosphere.

The significance of the polymer role in the formation of the composite is not only limited to the facilitation of the redox reaction. The polymer also acts as a separating agent during the high-temperature treatment. As mentioned above, at elevated temperatures, the polymer undergoes a transformation, resulting in the formation of a solid porous amorphous carbon matrix. The carbon matrix effectively prevents the Ni_2P particles from agglomerating and sintering, even at the high temperature of 1000°C. As a result, the individual phosphide particles with the size range varying from 5 to 200 nm remain well-dispersed and immobilized within the carbon matrix of the composite.

The surface area and porosity of the Ni_2P/C composite were evaluated before and after grinding. According to the results (Table 1), the total surface area of the composite increases from 344 to 366 $m^2 g^{-1}$ (equivalent BET surface area) or from 331.2 to 371.8 $m^2 g^{-1}$ (DFT cumulative surface area). In general, the shape of the recorded adsorption/desorption isotherms is typical for a microporous material that shows a step increase of the adsorbed volume below 0.05 P/P_0 associated with the filling of the micropore volume with the adsorbate (Fig. 6a). Such a shape of isotherms, which is specific for microporous materials, was previously reported for composites with similar composition only in a few studies[18,33]. Typically, Ni_2P hybrid materials obtained by other methods develop a nonporous or mesoporous structure with a surface area in the range of 6-455 $m^2 g^{-1}$ and an average of 166.9 $m^2 g^{-1}$ [4,7,13,17–20,22]. The pore size distribution of the composite before and after grinding is also shown in Figure 6b and 6c, respectively (DFT method). The result confirms the microporous structure of the composite where the pores with a diameter of 1-1.2 nm (half pore width 5-6 Å) make the main contribution to the pore volume. The grinding procedure results in mechanical impact on the structure, which on one hand increases micropore volume while on the other hand destroys the mesopores with a half-pore radius of 25-30 Å. The latter is evident not only from the DFT pore distribution analysis, but also from the change in the shape of the adsorption/desorption isotherm (Fig. 6a): the isotherm of the sample before grinding clearly shows a hysteresis loop that indicates the presence of mesopores, whereas after grinding the width of the loop is significantly reduced. As result, an insignificant decrease of the cumulative pore volume from 0.203 to 0.195 $cm^3 g^{-1}$ is provided by DFT calculation (Table 1).

In addition to BET and DFT analyses, the MP method based on statistical thickness analysis (t-plot) was used for sample characterisation[34]. The t-plot of the Ni_2P/C composite is shown in Figure 6d. The plot can be divided into two linear areas with different slopes. The first part of the t-plot has a sharp slope that appears in the early stage of adsorption when the adsorbed amount drastically increases on account of the micropore filling, but the statistical thickness of the adsorption does not increase so quickly. The plotted linear approximation curves do not intersect the origin (Fig 6d), which indicates the presence of non-accessible ultra-micropores with half pore width smaller than 3.5 Å. In this case, the Y-intercept values correlate with the volume of the ultra-micropores, which is increased after grinding (Table 1), however, the slope of the curves could not provide reliable information regarding the total surface area. The next linear area of the t-plot with a lower slope appears when adsorption into the micropores is complete and the next adsorption continues only on the external surface (outside micropores). The Y-intercept of the second linear approximation provides information regarding the total volume of the micropores. Accordingly, after grinding, the volume of the micropores increases from 0.165 to 0.181 $cm^3 g^{-1}$. The micropore size distribution of the composite indicates the presence of uniform micropores with half pore width of 5-6 Å, which volume slightly increases after grinding (Figure 6e and 6f). The value of the statistical thickness at the intersection point of the two linear approximations (5 Å) corresponds to the micropore openings' radius (half pore width). The slope value of the second linear approximation provides information about the external surface area, which constitutes only 10.4 $m^2 g^{-1}$ (Table 1). Accordingly, the high surface area of the composites can be attributed mainly to the contribution of the micropore surface area, whereas the contribution of the external surface area is only about 3%. After grinding, the external surface area

almost does not change whereas the micropore surface area increases 333.5 to 355.2 $m^2 g^{-1}$. Thus, the grinding of the composite results mainly in the opening of the closed microporosity channels.

Table 1. Surface area and pore size distribution analysis of the Ni_2P/C composite before and after grinding.

Ni_2P/C	before grinding	after grinding*
Surface area, $m^2 g^{-1}$		
Equivalent BET area	343.9	366.3
DFT cumulative surface area	331.2	371.8
t-plot method external surface area	10.4	11.1
Micropore surface area	333.5	355.2
Pore volume data, $cm^3 g^{-1}$		
DFT method cumulative pore volume (micropores and mesopores)	0.203	0.195
t-plot method (ultra-micropores)	0.025	0.034
t-plot method (micropores)	0.165	0.181

*planetary ball mill, 30 min, 60 rpm in ethanol

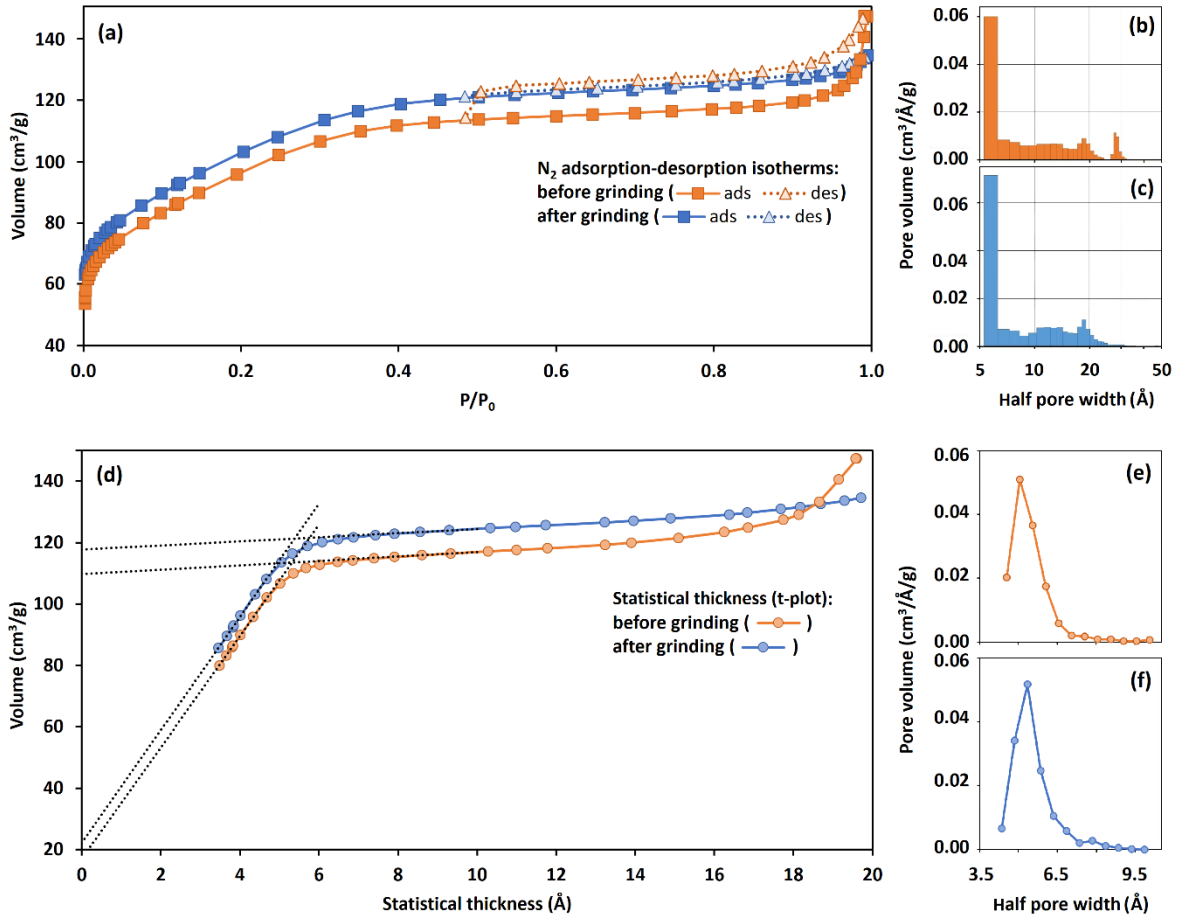

Figure 6. Surface properties of the Ni_2P/C composite before and after grinding: (a) N_2 adsorption/desorption isotherms; (b) pore size distribution histogram (DFT method) before grinding; (c) pore size distribution histogram (DFT method) after grinding; (d) statistical thickness (t-plot); (e) pore size distribution (MP method) before grinding; (f) pore size distribution (MP method) after grinding.

Evaluation of the apparent particle density of the composite before and after grinding indicates an insignificant increase in density from 3.4 to 3.7 g cm^{-3}. The volume of the material that is included in the calculation of the apparent particle density corresponds to a solid material volume and a closed pore volume with no openings, which cannot be filled with gas (He). Thus, the change in density after grinding can be attributed to the opening of the closed pore volume, which is also in agreement with the detected porosity changes. The density value can also be used for indirect calculation of the ratio between the carbon and phosphide parts of the composite. Considering that the theoretical density of Ni_2P is 7.36 and the density of amorphous carbon with prevailing sp^2 hybridisation is close to 1.5 g cm^{-3} [35], the Ni_2P content in the synthesised composite must be around 37%. The value is very close to that provided by the EDX analysis (40%wt).

3.2 Thermal and chemical stability of the Ni_2P/C composite

According to the DSC-TGA results (Fig. 7a), the thermal stability of the Ni_2P/C composite strongly depends on the atmosphere. With heating in an inert atmosphere, the composite slowly losses weight that is accelerated at 800-900 °C and results in a step-like weight loss effect accompanied by a strong endothermic effect. The process is significantly delayed with a heating rate increase from 1 to 10 °C min^{-1}. The weight loss effect is similar to that observed for the dried precursor (Fig. 5) and could indicate the same process. The most probably, the process is related to the pyrolysis of the polymer residues because the signals do not appear after repeated heating to the sample to these temperatures. The second endothermic effect at 1090 °C, which does not depend on the heating rate and is not accompanied by any weight change, corresponds to the melting of Ni_2P (T_m = 1100 °C, [36]). Heating of the sample above its melting temperature up to 1200 °C results upon cooling in recrystallisation of two nickel (II) phosphides (Ni_2P and $Ni_{12}P_5$) and graphite (C). The sample's composition after heating to 1200 °C in Ar (estimated on the basis of EDX, RIR and TGA) and its XRD pattern are shown in Fig. 7a and 7b, respectively. Thus, the inert atmosphere allows maintenance of the Ni_2P structure up to its melting point (1100 °C). On the contrary, in an oxidizing atmosphere, the sample behaves totally different, and its oxidation intensively starts already at 500-600 °C accompanied by multiple exothermic effects. The TGA study also reveals that at lower temperatures, oxidation is accompanied by substantial weight loss, whereas at higher temperatures - by the weight gain. Therefore, the low-temperature process can be connected with the oxidative decomposition of the carbon matrix whereas the high-temperature process - with the oxidation of the inorganic part, i.e. the transformation of Ni_2P to $Ni_3(PO_4)_2$ and NiO, as evidenced by XRD analysis (Fig. 7b). The complete oxidation of the Ni_2P phase is also evidenced by the absence of the melting effect of Ni_2P on the recorded DCS curve (Fig. 7a). Based on the results, the thermal stability of the sample is even in an oxidising atmosphere more than sufficient for many electrochemical applications, including HER electrocatalysis.

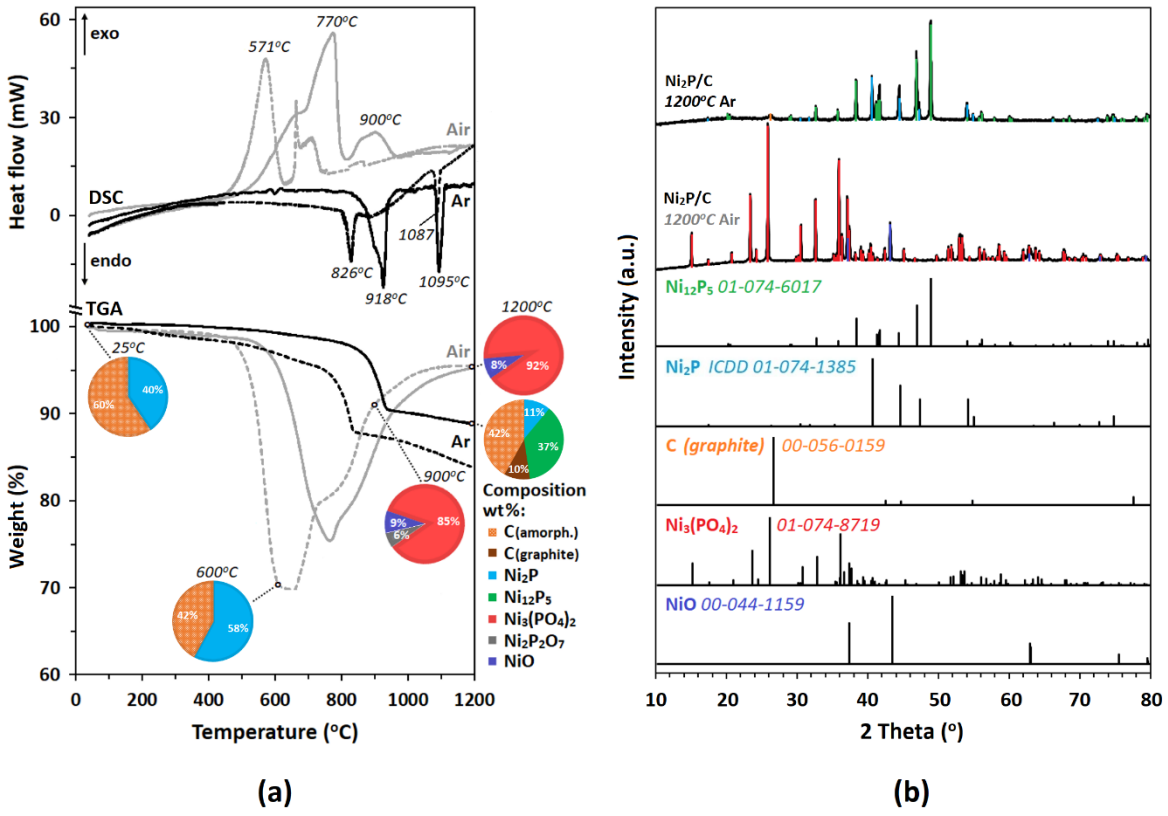

Fig 7. Thermal stability of the Ni_2P/C composite in an inert and oxidising atmosphere: (a) DSC-TGA curves in black correspond to an inert atmosphere (Ar), in green – to an oxidising atmosphere (air); the heating rate 10 °C min^{-1} - solid lines, 1 °C min^{-1} - dashed lines; pie charts show estimated quantitative composition (wt%), estimated on the basis of EDX, RIR and TGA; (b) XRD patterns of the samples after heating to 1200 °C in an inert and oxidising atmosphere.

The stability tests of the composite against aggressive chemical compounds (strong acids and bases) show no release of Ni- or phosphate-ions to the leaching solution. The results indicate an excellent chemical stability of the composite, which enables its application in the alkaline environment required for alkaline water electrolysis.

3.3 Catalytic activity of the Ni_2P/C composite in HER

Due to the excellent prospects of the studied phosphide composite for water splitting catalysis, its HER catalytic activity before and after grinding was investigated through electrochemical tests. The results clearly demonstrate a significant influence of the grinding procedure on the sample's activity (Fig. 8a, Table 2). The Tafel slope for ground Ni_2P/C, close to 120 mV dec^{-2} (Fig. 8b), indicates that the Volmer step (water dissociation and hydrogen adsorption) is the rate determining step[37]. The obtained even higher value of the Tafel slope can be attributed to a combination of several factors. Firstly, it can be associated with a greater coverage of the catalyst surface with adsorbed species, which is a result of the enhanced dissociation step facilitated by the partially negative P atoms that may weaken H—OH bond[38]. Additionally, in an alkaline environment, unlike in an acid one where only H^+ species can be adsorbed on the surface, the OH^- species can also block the active sites, further impacting the Tafel slope value. Furthermore, the presence of oxidized species on the catalyst surface might also contribute to an additional potential drop, resulting in overall higher Tafel slope value[39]. The overpotential needed to achieve 10 and 300 mA cm^{-2} decreases by approximately 100 and 200 mV, respectively (Table 2). As already mentioned, after the grinding, the micropore volume and micropore

surface area of the composite significantly increased, which could provide more active sites for the HER to occur. Thus, the available microporosity directly correlates with the catalytic activity of the studied composite suggesting that the Ni_2P particles are readily accessible through the opened micropores within the carbon matrix. Even though the values of overpotentials are among the higher reported in the literature[1], it should be noted that the composite consists of only 40% of active Ni_2P. Moreover, when compared to commercial Ni powder measured with the same procedure, ground Ni_2P/C exhibits superior activity (approximately 200 and 300 mV lower overpotentials for 10 and 300 mA cm^{-2}, respectively). These results, together with the optimised preparation method, suggest that the Ni_2P/C composite represents a promising material as a cathode catalyst in alkaline water electrolysis.

The results of the stability testing procedure of ground Ni_2P/C are shown in Figs. 8c,d. As expected, the HER polarisation resistance decreases with increasing potential that serves as a driving force to allow the HER to procced faster. Fig. 8c shows a gradual increase of the polarisation resistances after cycling by approximately 13 to 19% for the selected potentials. This indicates gradual degradation of the catalyst, at least to some extent. However, the decreasing values of the ohmic resistances during cycling suggest that delamination of the catalytic layer from the RDE surface could occur during the measurements (Supplement 3). This could also impact the values of polarisation resistance. Moreover, there is no noticeable shift in the measured polarisation curves after cycling (Fig. 8d). The overpotential at 10 mA cm^{-2} increased by only 7 mV (approximately 1.8%) for the sample before CV and after 1500 cycles. These results prove more than sufficient stability of the ground Ni_2P/C catalyst.

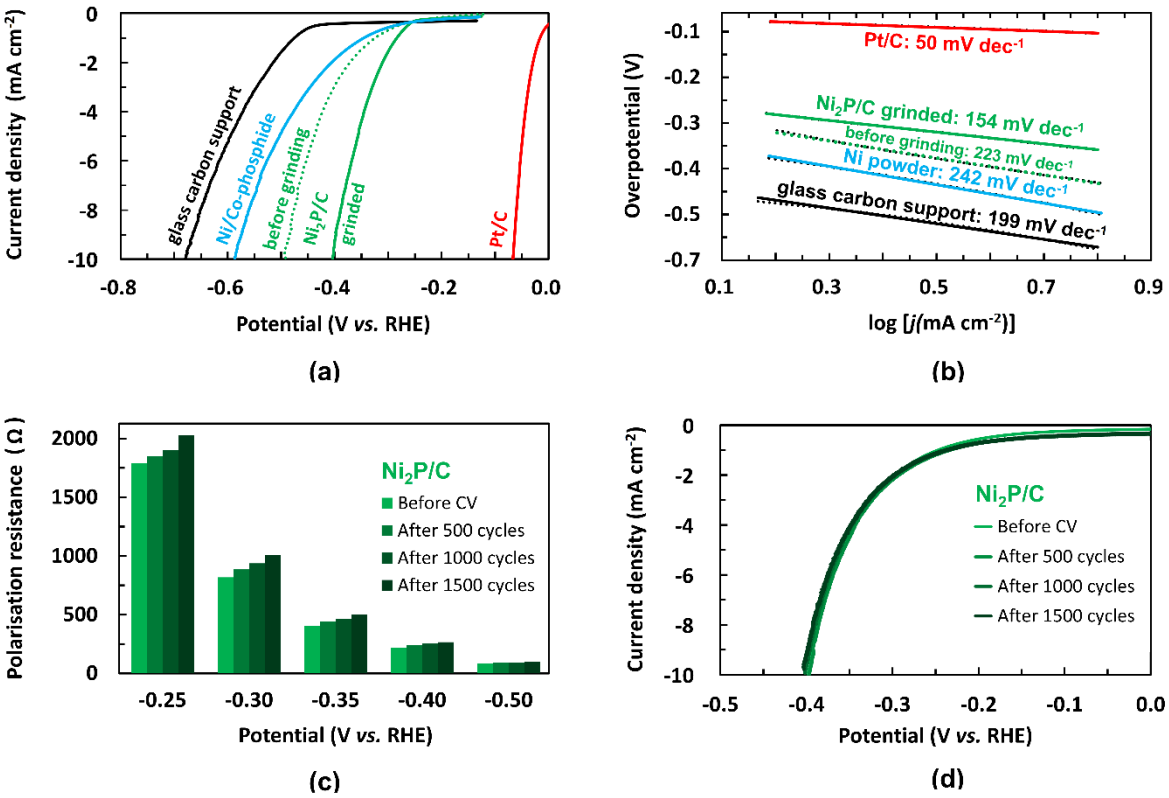

Figure 8. (a) HER polarisation curves and (b) the linear part of the Tafel plots of the selected samples. (c) HER polarisation resistance at different voltages and (d) HER polarisation curves of the ground Ni_2P/C catalyst before and after cyclic voltammetry tests. All curves are IR-corrected.

Table 2. Evaluated Tafel parameters analysis for the synthesised composite (Ni_2P/C) before and after grinding compared to other catalysts.

Catalyst	Tafel slope, mV dec^{-1}	Overpotential, at 10 mA cm^{-2}, mV	Overpotential at 300 mA cm^{-2}, mV	Exchange current density, mA cm^{-2}
Ni_2P/C (before grinding)	223	493	823	0.06
Ni_2P/C (ground)	154	391	619	0.048
Pt/C	50	64	137	0.514
Ni powder	242	573	931	0.043
Glass carbon support	199	653	947	0.005

4 Conclusions

This work presents an alternative method for the fabrication of highly efficient HER electrocatalyst based on crystalline Ni_2P suspended within an amorphous carbon matrix. The formation of the microporous Ni_2P/C composite was successfully achieved by a polymeric precursor method using inexpensive and stable compounds. Thermal analysis of the precursor and final product showed that the formation of Ni_2P depends on the type of atmosphere and that the Ni_2P/C composite even in the oxidizing atmosphere has sufficient thermal stability for electrochemical applications, including HER electrocatalysis. Furthermore, the grinding procedure increases the micropore surface area of the composite by opening the closed microporosity channels, leading to an increase in the number of catalytically active sites and enhancing the HER activity of the sample. The ground composite exhibited promising HER activity and great stability under alkaline water electrolysis conditions. The findings of this study highlight the importance of developing alternative preparation methods for HER catalysts, which can have a significant impact on the practical implementation and advancement of the hydrogen economy scheme. The as-prepared material holds great promise not only for the development of low-cost electrocatalysts for efficient water electrolysis but also for other application areas of transition metal phosphides.

Conflict of interests

There are no conflicts to declare.

Acknowledgments

SEM and IR measurements were financed by the project LM2023037. The authors also thank to Ministry of Education, Youth and Sports of the Czech Republic for the financial support of XPS measurements performed at CEMNAT (project LM 2018103).

References

1. M. Ďurovič, J. Hnát, and K. Bouzek: Electrocatalysts for the hydrogen evolution reaction in alkaline and neutral media. A comparative review. *J. Power Sources* **493**, 229708 (2021).

2. S. Liu, Y. An, Y. Liu, and Y. Xu: One-step construction of Ni_2P/GN and its superior energy storage performances. *Ionics (Kiel).* **26**(2), 849 (2020).

3. S. Yamaguchi, S. Fujita, K. Nakajima, S. Yamazoe, J. Yamasaki, T. Mizugaki, and T. Mitsudome: Support-boosted nickel phosphide nanoalloy catalysis in the selective hydrogenation of

maltose to maltitol. *ACS Sustain. Chem. Eng.* **9**, 6347 (2021).

4. H. Jiang, Y. Zhou, H. Zhu, F. Qin, Z. Han, M. Bai, J. Yang, J. Li, B. Hong, and Y. Lai: Interconnected stacked hollow carbon spheres uniformly embedded with Ni_2P nanoparticles as scalable host for practical Li metal anode. *Chem. Eng. J.* **428**, 132648:1 (2022).

5. W. Dai, H. Wen, Z. Zhang, and P. Wang: Metal-organic frameworks-derived Ni_2P@C Nanocomposite as a high-performance catalyst for hydrazine electrooxidation. *J. Alloys Compd.* **902**, 163746:1 (2022).

6. Y. Yu, Q. Chen, J. Li, P. Rao, R. Li, Y. Du, C. Jia, W. Huang, J. Luo, P. Deng, Y. Shen, and X. Tian: Progress in the development of heteroatom-doped nickel phosphates for electrocatalytic water splitting. *J. Colloid Interface Sci.* **607**, 1091 (2022).

7. Q. Wang, Z. Liu, H. Zhao, H. Huang, H. Jiao, and Y. Du: MOF-derived porous Ni_2P nanosheets as novel bifunctional electrocatalysts for the hydrogen and oxygen evolution reactions. *J. Mater. Chem. A* **6**, 18720 (2018).

8. M. Ďurovič, J. Hnát, M. Strečková, and K. Bouzek: Efficient cathode for the hydrogen evolution reaction in alkaline membrane water electrolysis based on NiCoP embedded in carbon fibres. *J. Power Sources* **556**, 232506 (2023).

9. E. J. Popczun, J. R. McKone, C. G. Read, A. J. Biacchi, A. M. Wiltrout, N. S. Lewis, and R. E. Schaak: Nanostructured nickel phosphide as an electrocatalyst for the hydrogen evolution reaction. *J. Am. Chem. Soc.* **135**(25), 9267 (2013).

10. R. B. Wexler, J. Mark, P. Martirez, and A. M. Rappe: Active role of phosphorus in the hydrogen evolving activity of nickel phosphide (0001) surfaces. *ACS Catal.* **7**, 7718 (2017).

11. L. Wu, L. Yu, F. Zhang, B. McElhenny, D. Luo, A. Karim, S. Chen, Z. Ren, L. B. Wu, L. Yu, F. H. Zhang, B. McElhenny, D. Luo, S. Chen, Z. F. Ren, and A. Karim: Heterogeneous bimetallic phosphide Ni_2P-Fe_2P as an efficient bifunctional catalyst for water/seawater splitting. *Adv. Funct. Mater.* **31**(1), 2006484 (2021).

12. G. E. Ayom, M. D. Khan, J. Choi, R. K. Gupta, W. E. Van Zyl, and N. Revaprasadu: Synergistically enhanced performance of transition-metal doped Ni_2P for supercapacitance and overall water splitting. *Dalt. Trans.* **50**, 11821 (2021).

13. S. Riyajuddin, K. Azmi, M. Pahuja, S. Kumar, T. Maruyama, C. Bera, and K. Ghosh: Super-hydrophilic hierarchical Ni-foam-Graphene-Carbon nanotubes-Ni_2P−CuP_2 nano-architecture as efficient electrocatalyst for overall water splitting. *ACS Nano* **15**, 5599 (2021).

14. X. Liang, B. Zheng, L. Chen, J. Zhang, Z. Zhuang, and B. Chen: MOF-derived formation of Ni_2P−CoP bimetallic phosphides with strong interfacial effect toward electrocatalytic water splitting. *ACS Appl. Mater.* **9**, 23222 (2017).

15. L. Xiong, B. Wang, H. Cai, H. Hao, J. Li, T. Yang, and S. Yang: Understanding the doping effect on hydrogen evolution activity of transition-metal phosphides: Modeled with Ni_2P. *Appl. Catal. B Environ.* **295**, 120283:1 (2021).

16. S. Huo, S. Yang, Q. Niu, F. Yang, and L. Song: Synthesis of functional Ni_2P/CC catalyst and the robust performances in hydrogen evolution reaction and nitrate reduction. *Int. J. Hydrogen Energy* **45**(7), 4015 (2020).

17. U. P. Suryawanshi, U. V Ghorpade, D. Min Lee, M. He, S. Wook Shin, P. V Kumar, J. Sung Jang, H. Rim Jung, M. P. Suryawanshi, and J. Hyeok Kim: Colloidal Ni_2P nanocrystals encapsulated in heteroatom-doped graphene nanosheets: a synergy of 0D@2D heterostructure toward overall water splitting. *Cite This Chem. Mater* **33**, 245 (2021).

18. X. Yan, S. Che, F. Yang, Z. Xu, H. Liu, C. Li, L. Yan, N. Ta, S. Sun, Q. Wei, L. Fang, and Y. Li: Highly

efficient water splitting catalyst composed of N,P-doped porous carbon decorated with surface P-enriched Ni_2P nanoparticles. *ACS Appl. Mater.* **14**, 20358 (2022).

19. Y. Yang, P. Zhang, Y. Lei, C. Zhou, J. Liu, S. Guo, S. Li, and L. Chen: In situ growth of nickel phosphide nanoparticles on inner wall of graphitic carbon nitride tubes for efficient photocatalytic hydrogen evolution. *Int. J. Hydrogen Energy* **46**(17), 10346 (2021).

20. F. Xu, Q. Xia, G. Du, Z. Fan, and N. Chen: Coral–like Ni_2P@C derived from metal–organic frameworks with superior electrochemical performance for hybrid supercapacitors. *Electrochim. Acta* **380**, 138200:1 (2021).

21. G. Li, S. Liu, D. Liu, and N. Zhang: MOF-derived porous nanostructured Ni_2P/C material with highly sensitive electrochemical sensor for uric acid. *Inorg. Chem. Commun.* **130**, 108713:1 (2021).

22. Y. Lu, X. L. Wang, X. Ge, X. Y. Zhao, T. Q. Wang, S. Huang, C. D. Gu, J. P. Tu, and S. X. Mao: Graphene-wrapped Ni_2P materials: a 3D porous architecture with improved electrochemical performance. *J. Solid State Electrochem.* **8**(18), 2245 (2014).

23. T. Liu, Q. Liu, A. M. Asiri, Y. Luo, and X. Sun: An amorphous CoSe film behaves as an active and stable full water-splitting electrocatalyst under strongly alkaline conditions. *ChemComm* **51**, 16683 (2015).

24. P. E. R. Blanchard, A. P. Grosvenor, R. G. Cavell, and A. Mar: X-ray photoelectron and absorption spectroscopy of metal-rich phosphides M_2P and M_3P (M = Cr-Ni). *Chem. Mater.* **20**, 7081 (2008).

25. Y. Zhao, Y. Zhao, H. Feng, and J. Shen: Synthesis of nickel phosphide nano-particles in a eutectic mixture for hydrotreating reactions. *J. Mater. Chem.* **21**, 8137 (2011).

26. W. Jastrzbski, M. Sitarz, M. Rokita, and K. Bułat: Infrared spectroscopy of different phosphates structures. *Spectrochim. Acta - Part A Mol. Biomol. Spectrosc.* **79**(4), 722 (2011).

27. F. Fievet, S. Ammar-Merah, R. Brayner, F. Chau, M. Giraud, F. Mammeri, J. Peron, J. Y. Piquemal, L. Sicard, and G. Viau: The polyol process: a unique method for easy access to metal nanoparticles with tailored sizes, shapes and compositions. *Chem. Soc. Rev.* **47**(14), 5187 (2018).

28. S. Khedri and S. Elyasi: Determination of the heat of pyrolysis of HDPE via isothermal differential scanning calorimetry: A new approach for solid state reactions. *J. Therm. Anal. Calorim.* **131**(2), 1509 (2018).

29. J. Gopalakrishnan, S. Pandey, and K. K. Rangan: Convenient route for the synthesis of transition-metal pnictides by direct reduction of phosphate, arsenate, and antimonate precursors. *Chem. Mater.* **9**, 2113 (1997).

30. R. Wang and K. J. Smith: The effect of preparation conditions on the properties of high-surface area Ni_2P catalysts. *Appl. Catal. A Gen.* **380**(1–2), 149 (2010).

31. N. Gorodylova and P. Šulcová: Polymerizable precursor method vs solid state reaction for the synthesis of $Ni_3(PO_4)_2$ yellow hue pigment with advanced characteristics. *J. Alloys Compd.* **903** (2022).

32. H. Aziam, S. Indris, M. Knapp, H. Ehrenberg, and I. Saadoune: Synthesis, characterization, electrochemistry, and in situ X-ray diffraction investigation of $Ni_3(PO_4)_2$ as a negative electrode material for lithium-ion batteries. *ChemElectroChem* **7**(18), 3866 (2020).

33. Z. Yan, Z. Sun, K. Yue, A. Li, and L. Qian: One-pot preparation of Ni_2P nanoparticles anchored on N, P co-doped porous carbon nanosheets for high-efficiency lithium storage. *J. Alloys Compd.* **877**, 160261:1 (2021).

34. R. S. Mikhail, S. Brunauer, and E. E. Bodor: Investigations of a complete pore structure analysis: I. Analysis of micropores. *J. Colloid Interface Sci.* **26**(1), 45 (1968).

35. L. Liu, F. Lu, J. Tian, S. Xia, and Y. Diao: Electronic and optical properties of amorphous carbon with different sp^3/sp^2 hybridization ratio. *Appl. Phys. A Mater. Sci. Process.* **125**(5), 1 (2019).

36. D. R. Lide: CRC Handbook of Chemistry and Physics, 79th Editi (CRC Press, Boca Raton, 1998).

37. B. E. Conway and B. V. Tilak: Interfacial processes involving electrocatalytic evolution and oxidation of H_2, and the role of chemisorbed H. *Electrochim. Acta* **47**(22–23), 3571 (2002).

38. Z. Rui, X. Wang, S. Yu, T. Wen, X. Zhu, F. Yang, X. Sun, X. Wang, and H. Wenping: Ternary $NiCo_2P_x$ nanowires as pH-universal electrocatalysts for highly efficient hydrogen evolution reaction. *Adv. Mater.* **29**(1605502), 1 (2017).

39. J. M. Jakšić, M. V. Vojnović, and N. V. Krstajić: Kinetic analysis of hydrogen evolution at Ni-Mo alloy electrodes. *Electrochim. Acta* **45**(25–26), 4151 (2000).